Chiral response in lattice models of Weyl materials

E. V. Gorbar, V. A. Miransky, I. A. Shovkovy, and P. O. Sukhachov

Phys. Rev. B **96**, 125123 — Published 15 September 2017

DOI: 10.1103/PhysRevB.96.125123

Chiral response in lattice models of Weyl materials

E. V. Gorbar,[1,2] V. A. Miransky,[3] I. A. Shovkovy,[4,5] and P. O. Sukhachov[3]

[1]*Department of Physics, Taras Shevchenko National Kiev University, Kiev, 03680, Ukraine*
[2]*Bogolyubov Institute for Theoretical Physics, Kiev, 03680, Ukraine*
[3]*Department of Applied Mathematics, Western University, London, Ontario N6A 5B7, Canada*
[4]*College of Integrative Sciences and Arts, Arizona State University, Mesa, Arizona 85212, USA*
[5]*Department of Physics, Arizona State University, Tempe, Arizona 85287, USA*

For a generic lattice Hamiltonian of the electron states in Weyl materials, we calculate analytically the chiral (or, equivalently, valley) charge and current densities in the first order in background electromagnetic and strain-induced pseudoelectromagnetic fields. We find that the chiral response induced by the pseudoelectromagnetic fields is not topologically protected. Although our calculations reproduce qualitatively the anomalous chiral Hall effect, the actual result for the conductivity depends on the definition of the chirality as well as on the parameters of the lattice model. In addition, while for the well-separated Fermi surfaces surrounding the individual Weyl nodes the current induced by the magnetic field coincides almost exactly with the current of the chiral separation effect, there are clear deviations when the Fermi surfaces undergo the Lifshitz transition. Moreover, we found that all chiral response coefficients vanish at large chemical potential.

I. INTRODUCTION

The study of Weyl semimetals [1–9], where quasiparticles are described by the relativistic-like Weyl equations in the vicinity of Weyl nodes, has attracted a lot of attention in recent years. Note that while the Standard Model of elementary particles has particles (neutrinos) of only one chirality, this is impossible in lattice models. Indeed, as was proved by Nielsen and Ninomiya [10], particle species in the lattice models must always come in pairs of opposite chirality. This theorem is directly relevant for the low-energy spectrum of Weyl materials characterized by the Weyl nodes separated in the momentum space $\mathbf{b}$ and/or energy b_0 [1–9]. This separation makes these materials qualitatively different from the Dirac materials, in which Weyl nodes of opposite chiralities overlap [11–20].

Because of a nontrivial Berry curvature [21] associated with monopole-like sources of the topological charge at the Weyl nodes, Weyl materials have interesting transport properties [22–33]. Among other things, they include the anomalous quantum Hall effect [22–27] and the chiral magnetic effect [32, 33] (introduced first in the high energy physics context in Ref. [34]), which are associated with the electric currents in background electromagnetic fields. The corresponding currents are proportional to the momentum $\mathbf{b}$ and energy b_0 separations between the Weyl nodes, respectively. Note that the chiral magnetic effect is absent in the equilibrium state of Weyl materials in a magnetic field as required by the standard notions of the solid state physics [32].

The chiral kinetic theory [35–37] is an efficient approach to study the electromagnetic response of Weyl matter, including the effects due to the chiral anomaly [38] in background electromagnetic fields. However, the conventional formulation [35–37] of the chiral kinetic theory has a serious limitation. It does not depend on the momentum $\mathbf{b}$ or energy b_0 separation between the Weyl nodes and, therefore, cannot capture all topological currents. In fact, it misses the Bardeen-Zumino-Chern-Simons (BZCS) current [39, 40], which is critical for the accurate description of both the chiral magnetic effect [32, 33] and the anomalous Hall effect [22–27]. In addition, the importance of the BZCS current is clearly manifested in collective excitations in Weyl matter [41, 42]. Note that the corresponding term [43] was first introduced in relativistic quantum field theory in order to define the consistent anomaly. In our recent paper [44], we demonstrated that the BZCS current appears automatically in lattice models of Weyl materials and is connected with the winding number of the mapping of a two dimensional section of the Brillouin zone onto the unit sphere.

In Refs. [39, 40] it was argued that, in addition to the BZCS terms in the electric charge and current densities, their chiral or axial counterparts should be also accounted for. In the four-vector notation, the corresponding chiral BZCS current is given by $j^{\nu}_{5,\,\mathrm{BZCS}} = -e^2\epsilon^{\nu\rho\alpha\beta}A^5_\rho F^5_{\alpha\beta}/(12\pi^2\hbar^2 c)$, where $A^5_\rho = b_\rho + \tilde{A}^5_\rho$. Here $b_\rho = (b_0, -\mathbf{b})$ and $\tilde{A}^5_\rho$ is an axial gauge field. In Weyl materials, the latter can be induced, in general, by strains [45–51]. This was explicitly shown using the tight-binding lattice models in Refs. [47, 48]. Static strains, in particular, could produce background pseudomagnetic fields, $\mathbf{B}_5 = \boldsymbol{\nabla}\times\mathbf{A}_5$. Pseudoelectric fields $\mathbf{E}_5$, on the other hand, could be induced by dynamical deformations. Unlike the ordinary electromagnetic fields, the pseudoelectromagnetic ones couple to opposite chirality quasiparticles with different sign.

In this paper, we study how the topology affects the chiral (or, equivalently, valley) charge and current densities in Weyl materials. The first studies of the valley currents were done in Ref. [45] by using the chiral kinetic theory. By noting that an applied magnetic field can produce a valley current, it was suggested there that the Weyl semimetals might be good candidates for valleytronics. Notably, the majority of the previous attempts to utilize the valley

degree of freedom were primarily focusing on 2D systems such as graphene [52–54] and the monolayer molybdenum disulphide (MoS_2) [55, 56]. In these systems, the valley Hall effect is realized by the edge state carriers moving in opposite directions in different valleys when an in-plane electric field is applied.

To the best of our knowledge, there are no explicit calculations of the chiral current and valley polarization (chiral charge) densities in lattice models of Weyl matter. The only lattice studies we are aware of are related to the investigation of the chiral separation effect in a relativistic Dirac plasma [57–59]. However, it is still unknown whether the chiral analog of the BZCS term can be derived in the lattice models and whether it enjoys the same topological robustness as its counterpart in the electric current. These questions provide the main motivation and will be systematically addressed in this paper.

This paper is organized as follows. We introduce in Sec. II a generic lattice model of Weyl matter and outline the formalism that will be used to study the chiral response. In Secs. III and IV, we calculate the chiral charge and current densities in the linear order in background magnetic and electric fields, respectively. The response to strain-induced pseudoelectromagnetic fields in Weyl materials is studied in Sec. V. We summarize and discuss our results in Sec. VI. Technical details of derivations are presented in several appendices at the end of the paper. Throughout the paper, we use the units with $\hbar = c = 1$.

II. MODEL

We consider a generic lattice model of Weyl materials defined by the following Hamiltonian [22, 32]:

$$\mathcal{H}_{\rm latt} = d_0 + \mathbf{d}\cdot\boldsymbol{\sigma}, \tag{1}$$

where $\boldsymbol{\sigma} = (\sigma_x, \sigma_y, \sigma_z)$ are the Pauli matrices and functions d_0 and $\mathbf{d}$ are periodic functions of the (quasi)momentum $\mathbf{k} = (k_x, k_y, k_z)$. Their explicit form is given by

$$d_0 = g_0 + g_1\cos(a_z k_z) + g_2\left[\cos(a_x k_x) + \cos(a_y k_y)\right], \tag{2}$$
$$d_1 = \Lambda\sin(a_x k_x), \tag{3}$$
$$d_2 = \Lambda\sin(a_y k_y), \tag{4}$$
$$d_3 = t_0 + t_1\cos(a_z k_z) + t_2\left[\cos(a_x k_x) + \cos(a_y k_y)\right], \tag{5}$$

where a_x, a_y, and a_z denote the lattice spacings and parameters g_0, g_1, g_2, Λ, t_0, t_1, and t_2 are material dependent. Their values are given in Appendix A. In order to simplify our analytical calculations, we will assume that the lattice is cubic, i.e., $a_x = a_y = a_z = a$. The model describes two Weyl nodes separated in momentum space by $\Delta k_z = 2b_z$ [see Eq. (A10)] and is symmetric with respect to the replacement $k_z \to -k_z$. As in Ref. [44], here we will consider a simplified version of model (1) with the vanishing value of d_0, which preserves all topological properties of the original model, but gets rid of the asymmetry between the valence and conduction bands (i.e., effectively enforces the particle-hole symmetry). Note that Hamiltonian (1) can be used to investigate response in the Weyl materials, as well as in truly relativistic Weyl matter. In the latter case, the value of $\Lambda \propto 1/a$ can be interpreted as an ultraviolet cut-off that should be taken to infinity at the end of calculations.

Before discussing the chiral charge and current densities in the lattice model of Weyl materials induced by background electromagnetic and pseudoelectromagnetic fields, it is necessary to emphasize from the very beginning that the concept of chirality is well-defined only for quasiparticles in the vicinity of the Weyl nodes, while its generalization to the whole Brillouin zone is problematic. This was known for a long time in the context of the lattice models of relativistic field theories, which were introduced by Wilson [60] as the only practical means of performing the first-principles calculations in gauge theories such as QCD (see, e.g., Refs. [61, 62]). According to the no-go theorem of Nielsen and Ninomiya [63], however, it is impossible to formulate a Hermitian, local, chirally symmetric theory on the lattice without fermion species doubling. This leads to the problems for numerical lattice simulations of the chiral gauge theories (such as the electroweak gauge theory, where the corresponding fermion representations are chiral). Nevertheless, by making use of the Ginsparg-Kaplan equation [64] for the lattice Dirac operator, it is possible to define a *modified* chiral symmetry which leaves the lattice action for massless fermions invariant. This equation quantifies to what extent the chiral symmetry could be implemented on the lattice in relativistic quantum field theories. The corresponding formulation is standard and used in the lattice simulations of the Standard Model fields.

In our study, we will consider two definitions of chirality. The first one is given by

$$\chi_1(\mathbf{k}) \equiv \operatorname{sgn}(v_x v_y v_z), \tag{6}$$

where $v_i \equiv \partial_{k_i} d_i$ is the quasiparticle velocity. This is the standard definition of chirality for systems with a linear dispersion law, i.e., $\mathcal{H} \sim \sum_{i=1}^{3} v_i k_i \sigma_i$, albeit generalized to the entire Brillouin zone. The second definition is specific

for the lattice model under consideration and is connected with the reflection symmetry $k_z \to -k_z$ of Hamiltonian (1), i.e.,

$$\chi_2(\mathbf{k}) \equiv -\operatorname{sgn}(k_z)\,. \tag{7}$$

The corresponding reflection symmetry can be identified with the existence of two valleys in model (1) and could be also viewed as a valley symmetry. Therefore, the definition of chirality in Eq. (7) makes sense even for the states far away from the Weyl nodes. Note, however, that it is limited only to Weyl materials with the broken time-reversal symmetry.

For the quasiparticle states with momenta in the vicinity of the Weyl nodes, both definitions of chirality in Eqs. (6) and (7) are completely equivalent. This will be also evident from the similarity of the matter contributions in the chiral response at small values of the chemical potential. In general, however, the two definitions differ for the states far from the Weyl nodes. Henceforth, in the rest of this paper, we use both definitions and compare the predictions that follow.

III. CHIRAL CHARGE AND CURRENT DENSITIES IN A BACKGROUND MAGNETIC FIELD

In this section we derive the explicit expressions for the chiral (or valley) charge and current densities to the linear order in a background magnetic field. We assume that the field points in the $+z$ direction and is described by the vector potential in the Landau gauge $\mathbf{A} = (0, xB, 0)$. The general expressions for the chiral charge and current densities in the model at hand are presented in Appendix B. Note that in the present paper we limit ourselves to the case of zero temperature $T \to 0$.

Let us start from the chiral charge density ρ^5. For the definition of the corresponding quantity in terms of the Green's function as well as some technical details of the derivation, see Appendix B. In order to separate the topological, i.e., independent of the chemical potential, and nontopological parts of ρ^5, let us first consider the case of the vanishing chemical potential $\mu = 0$, i.e.,

$$\rho^5_0 = -\frac{e^2}{(2\pi)^3}\int d^3\mathbf{k}\,\chi(\mathbf{k})\,(\mathbf{B}\cdot\mathbf{\Omega})\,, \tag{8}$$

where $\chi(\mathbf{k})$ is a momentum dependent chirality function which is given either by Eq. (6) or Eq. (7) and we used the following definition of the Berry curvature [65]:

$$\Omega_i = \sum_{l,m=1}^{3} \frac{\epsilon_{ilm}}{4}\left(\hat{\mathbf{d}}\cdot\left[(\partial_{k_l}\hat{\mathbf{d}})\times(\partial_{k_m}\hat{\mathbf{d}})\right]\right), \tag{9}$$

with $\hat{\mathbf{d}} \equiv \mathbf{d}/|\mathbf{d}|$. The Berry curvature can be also viewed as the Jacobian of the mapping of a two dimensional section of the Brillouin zone onto the unit sphere. When integrated over the area of the cross-section (i.e., the k_x-k_y plane), it counts the winding number of the mapping or the Chern number [66]

$$\mathcal{C}(k_z) = \frac{1}{2\pi}\int dk_x\,dk_y\,\Omega_z. \tag{10}$$

This Chern number $\mathcal{C}(k_z)$ depends on k_z and vanishes for $|k_z| \geq b_z$.

It is instructive to compare the result in Eq. (8) with the electric charge density obtained in Ref. [44]. The latter is given by a similar expression, but has no chirality multiplier $\chi(\mathbf{k})$ in the integrand. Because of the additional factor $\chi(\mathbf{k})$, the chiral charge density does not have the same topological robustness as the electric charge density. Nevertheless, it may be convenient to define a chiral analog of the Chern number,

$$\mathcal{C}_\chi(k_z) = \frac{1}{4\pi}\int dk_x\,dk_y\,\chi(\mathbf{k})\,\left(\hat{\mathbf{d}}\cdot\left[(\partial_{k_x}\hat{\mathbf{d}})\times(\partial_{k_y}\hat{\mathbf{d}})\right]\right). \tag{11}$$

In the case of the chirality defined by Eq. (7), i.e., $\chi(\mathbf{k}) \equiv \chi_2(\mathbf{k})$, there is a simple relation between the two Chern numbers: $\mathcal{C}_{\chi_2}(k_z) = -\operatorname{sgn}(k_z)\,\mathcal{C}(k_z)$. However, there is no simple relation between the Chern number and its chiral analog when the other definition of chirality (6), i.e., $\chi(\mathbf{k}) \equiv \chi_1(\mathbf{k})$, is used. This is due to the fact that $\chi_1(\mathbf{k})$ depends on all components of the momentum $\mathbf{k}$. The numerical comparison of the two chiral analogs of the Chern number, $\mathcal{C}_{\chi_1}$ and $\mathcal{C}_{\chi_2}$, is presented in the left panel of Fig. 1. As expected, $\mathcal{C}_{\chi_2}$ takes only integer values and is nonzero for

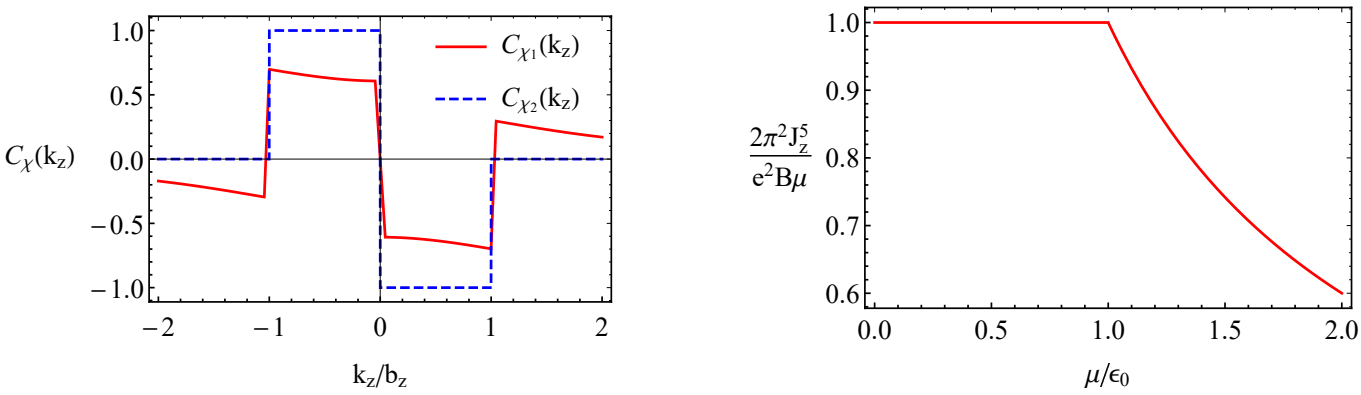

FIG. 1. Left: The chiral analog of the Chern number $\mathcal{C}_\chi(k_z)$ as a function of k_z/b_z. The results are shown for the two definitions of the chirality: $\chi(\mathbf{k}) = \chi_1(\mathbf{k})$ (red solid line) and $\chi(\mathbf{k}) = \chi_2(\mathbf{k})$ (dashed blue line). Right: The chiral current density J_z^5 measured in units of $J_{z,\mathrm{CSE}}^5$, see Eq. (15), as a function of μ/ϵ_0. The results in both panels are plotted for the numerical values of parameters defined in Appendix A.

$|k_z| < b_z$. In view of the reflection symmetry $k_z \to -k_z$ of model (1), $\mathcal{C}_{\chi_2}$ can be considered as a symmetry protected topological invariant. In contrast, $\mathcal{C}_{\chi_1}$ is generically noninteger and depends on the details of the model.

At nonzero chemical potential μ, the complete expression for the chiral charge density valid to the linear order in magnetic field $\mathbf{B}$ reads

$$\rho^5 = \rho_0^5 + \rho_\mu^5, \tag{12}$$

where the additional "matter" part of the density is given by

$$\rho_\mu^5 = e^2 \int \frac{d^3\mathbf{k}}{(2\pi)^3}\, \chi(\mathbf{k})\, (\mathbf{B}\cdot\mathbf{\Omega})\left[\theta\left(|\mu| - |\mathbf{d}|\right) + |\mathbf{d}|\,\delta\left(|\mu| - |\mathbf{d}|\right)\right]. \tag{13}$$

For a specific set of model parameters, it is straightforward to calculate the corresponding contribution to the charge density using numerical methods. After the integration over $\mathbf{k}$, we find that the total chiral charge density vanishes for both definitions of $\chi(\mathbf{k})$. Note that the absence of the "vacuum" part ρ_0^5 can be easily established from the asymmetry of the chiral Chern number, i.e., $C_\chi(k_z) = -C_\chi(-k_z)$. Therefore, no chiral charge is induced by a magnetic field.

Similarly, by making use of the results in Appendix B, we derive the following chiral current density:

$$J_n^5 = -e^2 B \int \frac{d^3\mathbf{k}}{(2\pi)^3}\, \chi(\mathbf{k})\, \mathrm{sgn}\,(\mu)\left((\partial_{k_n}\mathbf{d})\cdot\left[(\partial_{k_x}\mathbf{d})\times(\partial_{k_y}\mathbf{d})\right]\right)\delta\left(\mu^2 - |\mathbf{d}|^2\right). \tag{14}$$

After integrating over the Brillouin zone, we find that only the longitudinal component (with respect to $\mathbf{B}$) of the chiral current density is nonzero. Its dependence on the chemical potential is shown in the right panel of Fig. 1. Note that the horizontal axis shows the dimensionless ratio μ/ϵ_0, where $\epsilon_0 = \lim_{\mathbf{k}\to\mathbf{0}} |\mathbf{d}|$ is the height of the "dome" between the Weyl nodes in the energy spectrum. For sufficiently small values of the chemical potential, i.e., $|\mu| < \epsilon_0$, when two separate chiral sheets of the Fermi surface are formed, the chiral current density coincides with the well-known expression in linearized effective models

$$\mathbf{J}_{\mathrm{CSE}}^5 = -\frac{e^2\mathbf{B}\mu}{2\pi^2}. \tag{15}$$

This is nothing else but the conventional chiral separation effect [67, 68]. The dependence of the chiral current density changes, however, when $|\mu| > \epsilon_0$. As is easy to check, the corresponding qualitative change in the behavior is connected with a Lifshitz transition at $|\mu| = \epsilon_0$. Indeed, for chemical potentials larger than ϵ_0, the concept of chirality becomes ambiguous and, as a consequence, the chiral current gets reduced compared to the value given by Eq. (15). It is interesting to note that the results are almost the same for both definitions of the chirality. This is explained by the fact that, due to the presence of the δ-function, current (14) for small values of μ is determined by the states in the vicinity of Weyl nodes where $\chi_1(\mathbf{k}) \simeq \chi_2(\mathbf{k})$.

Let us briefly discuss the physical meaning of the chiral or valley current (14). In contrast to the electric current, the chiral one is not directly observable. However, an interplay between the electric and chiral currents produces

a new type of collective excitations known as a chiral magnetic wave [69]. In essence, the corresponding wave is a self-sustained mode in which the chiral current induces a fluctuation of the chiral chemical potential that drives the electric current via the chiral magnetic effect. The electric current, in turn, produces a fluctuation of the chemical potential that closes the cycle. The induced chiral current (14) also affects the properties of chiral plasmons in a qualitative way [41, 42]. Therefore, the detection of collective modes could provide an indirect observation of the chiral current.

IV. RESPONSE TO A BACKGROUND ELECTRIC FIELD

In this section we study the chiral response to a background electric field. By using the Kubo's linear response theory, one can write the chiral charge and current densities in the form $\rho^5 = \sigma^5_{0m} E_m$ and $J^5_n = \sigma^5_{nm} E_m$, respectively, where the generalized direct current (DC) chiral conductivity tensor $\sigma^5_{\nu m,\mathrm{tot}}$ is given by the following relation:

$$\sigma^5_{\nu m,\mathrm{tot}} = \lim_{\Omega\to 0} \frac{i}{\Omega} T \sum_{l=-\infty}^{\infty} \int \frac{d^3\mathbf{k}}{(2\pi)^3} \int\int d\omega d\omega' \frac{\mathrm{tr}\left[\chi(\mathbf{k})\, j_\nu(\mathbf{k}) A(\omega;\mathbf{k}) j_m(\mathbf{k}) A(\omega';\mathbf{k})\right]}{(i\omega_l + \mu - \omega)\,(i\omega_l - \Omega - i0 + \mu - \omega')}. \tag{16}$$

In the last expression, $\omega_l = (2l+1)\pi T$ (with $l \in \mathbb{Z}$) are the fermionic Matsubara frequencies, $A(\omega;\mathbf{k})$ is the spectral density defined in Eq. (A12), and $j_\nu = (e, e\boldsymbol{\nabla}_{\mathbf{k}}\mathcal{H}_{\mathrm{latt}})$.

Performing the summation over the Matsubara frequencies and setting $T = 0$, we derive the following result for the generalized chiral conductivity tensor:

$$\sigma^5_{0m} = e^2\pi \int \frac{d^3\mathbf{k}}{(2\pi)^3} \chi(\mathbf{k}) \frac{\delta^2_\Gamma(\mu - |\mathbf{d}|) - \delta^2_\Gamma(\mu + |\mathbf{d}|)}{|\mathbf{d}|} \left(\mathbf{d}\cdot\partial_{k_m}\mathbf{d}\right), \tag{17}$$

$$\tilde{\sigma}^5_{nm} = -e^2 \int \frac{d^3\mathbf{k}}{(2\pi)^3} \chi(\mathbf{k}) \frac{\left(\mathbf{d}\cdot[(\partial_{k_n}\mathbf{d})\times(\partial_{k_m}\mathbf{d})]\right)}{2|\mathbf{d}|^3} \left[1 - \theta(|\mu| - |\mathbf{d}|)\right], \tag{18}$$

$$\sigma^5_{nm} = 2e^2\pi \int \frac{d^3\mathbf{k}}{(2\pi)^3} \frac{\chi(\mathbf{k})}{4|\mathbf{d}|^2} \sum_{s,s'=\pm} \delta_\Gamma(\mu - s|\mathbf{d}|)\delta_\Gamma(\mu - s'|\mathbf{d}|) \Big\{ |\mathbf{d}|^2 \left[(\partial_{k_n}\mathbf{d})\cdot(\partial_{k_m}\mathbf{d})\right]$$
$$+ 2ss' \left[(\partial_{k_n}\mathbf{d})\cdot\mathbf{d}\right]\left[(\partial_{k_m}\mathbf{d})\cdot\mathbf{d}\right] - ss' \left[(\partial_{k_n}\mathbf{d})\cdot(\partial_{k_m}\mathbf{d})\right]|\mathbf{d}|^2 \Big\}, \tag{19}$$

where we separated the nondissipative $\tilde{\sigma}^5_{nm}$ and dissipative σ^5_{nm} contributions to the generalized chiral conductivity tensor. Such a separation is unambiguously done by studying the dependence on the phenomenologically introduced transport quasiparticle width $\Gamma(\mu)$. Indeed, the nondissipative (dissipative) part of the conductivity tensor is finite (divergent) in the limit $\Gamma(\mu) \to 0$. In a realistic model of a Weyl material, a nonzero quasiparticle width $\Gamma(\mu)$ may result, for example, from a short-range disorder. [For the key details of the derivation as well as for the definition of $\delta_\Gamma(x)$, see Appendix B 2.] For definiteness, we assume that the quasiparticle width in the model at hand is $\Gamma(\mu) = \Gamma_0(1 + \mu^2/\epsilon_0^2)$, which includes a constant part Γ_0 as well as a part determined by the density of states $\sim \mu^2$ [70].

After integrating over the Brillouin zone, we find that σ^5_{03} is the only nontrivial component of the generalized chiral conductivity tensor. This component describes the chiral charge density induced by the electric field. At $T = 0$, the numerical dependence of σ^5_{03} on the chemical potential is shown in Fig. 2 for several choices of the disorder strength Γ_0. Since the results are almost the same for both definitions of chirality $\chi_1(\mathbf{k})$ and $\chi_2(\mathbf{k})$, we present the results only for $\chi(\mathbf{k}) = \chi_2(\mathbf{k})$. As is evident from the dependence of the numerical results on the disorder strength, the chiral charge density is not topologically protected.

V. RESPONSE TO STRAIN-INDUCED PSEUDOELECTROMAGNETIC FIELDS

For completeness, in this section, we will also study the chiral response to pseudoelectromagnetic fields. This response is directly relevant for Weyl materials where pseudomagnetic $\mathbf{B}_5$ and pseudoelectric $\mathbf{E}_5$ fields could be induced by mechanical strains [45–51]. From the viewpoint of lattice simulations in high energy physics, this might be also of interest in connection with the chiral analog of the BZCS term. As we mentioned in the Introduction, this provides one of the main motivations for the present study.

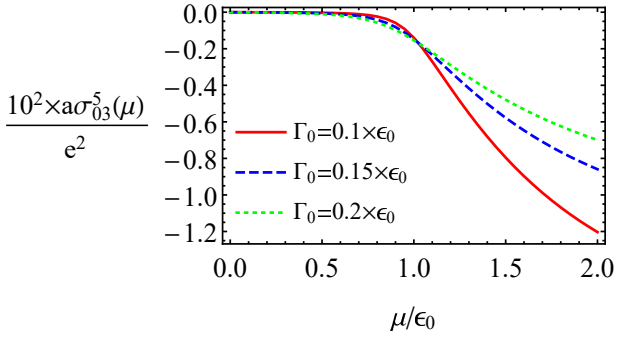

FIG. 2. The dependence of the generalized chiral conductivity σ_{03}^5 on μ/ϵ_0. The red solid, blue dashed, and green dotted lines correspond to $\Gamma_0 = 0.1\,\epsilon_0$, $\Gamma_0 = 0.15\,\epsilon_0$, and $\Gamma_0 = 0.2\,\epsilon_0$, respectively. The results are plotted for the model parameters given in Appendix A.

By making use of the results in Ref. [50], we will account for the effect of strains by including the following additional terms in the lattice Hamiltonian (1):

$$\delta h_{\rm strain} = \Lambda\left(u_{13}\sigma_x + u_{23}\sigma_y\right)\sin\left(ak_z\right) - t_1 u_{33}\sigma_z\cos\left(ak_z\right) \equiv \mathbf{A}_5\cdot\mathbf{j}^5, \tag{20}$$

where $u_{ij} = \left(\partial_i u_j + \partial_j u_i\right)/2$ is the strain tensor and $\mathbf{u}$ is the displacement vector. In components, the axial gauge potential and the operator of the strain-induced axial current density are given by

$$\mathbf{A}_5 = \frac{1}{ea}\left[u_{13}\sin\left(ab_z\right), u_{23}\sin\left(ab_z\right), u_{33}\cot\left(ab_z\right)\right] \tag{21}$$

and

$$\mathbf{j}^5 = ea\left(\frac{\Lambda\sin\left(ak_z\right)}{\sin\left(ab_z\right)}\sigma_x, \frac{\Lambda\sin\left(ak_z\right)}{\sin\left(ab_z\right)}\sigma_y, -\frac{t_1\cos\left(ak_z\right)}{\cot\left(ab_z\right)}\sigma_z\right), \tag{22}$$

respectively.

For example, a local pseudomagnetic field could be induced by a torsion with the displacement vector given by $\mathbf{u} = \theta z[\mathbf{r}\times\hat{\mathbf{z}}]/L$, where θ is the torsion angle and L is the length of the crystal. Then, the associated strain-induced pseudomagnetic field reads $\mathbf{B}_5 \equiv \boldsymbol{\nabla}\times\mathbf{A}_5 = -\theta/(Lea)\sin\left(ab_z\right)\hat{\mathbf{z}}$. On the other hand, a dynamical displacement with $\mathbf{u}\sim t$ gives rise to a uniform pseudoelectric field $\mathbf{E}_5 = -\partial_t\mathbf{A}_5$. Below, we briefly address both these possibilities.

A. Response to a pseudomagnetic field

In the full analogy to the case of an ordinary magnetic field, see Eqs. (B5) and (B6), the chiral charge and current densities in the background pseudomagnetic field are given by

$$\rho^5 = \frac{eB_5}{4}\int\frac{d\omega d^3\mathbf{k}}{(2\pi)^4}\chi(\mathbf{k})\,\mathrm{tr}\Big[-(\partial_{k_y}G^{(0)})j_x^5 G^{(0)} + G^{(0)}j_x^5(\partial_{k_y}G^{(0)}) + (\partial_{k_x}G^{(0)})j_y^5 G^{(0)} - G^{(0)}j_y^5(\partial_{k_x}G^{(0)})\Big], \tag{23}$$

$$\begin{aligned} J_n^5 = \frac{B_5}{4}\int\frac{d\omega d^3\mathbf{k}}{(2\pi)^4}\chi(\mathbf{k})\,\mathrm{tr}\Big[&-j_n(\partial_{k_y}G^{(0)})j_x^5 G^{(0)} + j_n G^{(0)}j_x^5(\partial_{k_y}G^{(0)}) - \delta_{n,y}(\partial_{k_y}j_y)G^{(0)}j_x^5 G^{(0)} - 2ir_n\delta_{n,y}j_y G^{(0)}j_x^5 G^{(0)} \\ &+ j_n(\partial_{k_x}G^{(0)})j_y^5 G^{(0)} - j_n G^{(0)}j_y^5(\partial_{k_x}G^{(0)}) + \delta_{n,x}(\partial_{k_x}j_x)G^{(0)}j_y^5 G^{(0)} + 2ir_n\delta_{n,x}j_x G^{(0)}j_y^5 G^{(0)}\Big], \end{aligned} \tag{24}$$

where the Green's function $G^{(0)}$ is defined in Eq. (A11). After the integration over ω, the above equations lead to the following "vacuum" and "matter" parts of the chiral charge density, respectively:

$$\rho_0^5 = \frac{e^2B_5a\Lambda}{4\sin\left(ab_z\right)}\int\frac{d^3\mathbf{k}}{(2\pi)^3}\frac{\sin\left(ak_z\right)}{|\mathbf{d}|^3}\chi(\mathbf{k})\left\{\left[(\partial_{k_y}\mathbf{d})\times\mathbf{d}\right]_x - \left[(\partial_{k_x}\mathbf{d})\times\mathbf{d}\right]_y\right\}, \tag{25}$$

$$\rho_\mu^5 = -\frac{e^2B_5a\Lambda}{4\sin\left(ab_z\right)}\int\frac{d^3\mathbf{k}}{(2\pi)^3}\frac{\sin\left(ak_z\right)}{|\mathbf{d}|^3}\chi(\mathbf{k})\left\{\left[(\partial_{k_y}\mathbf{d})\times\mathbf{d}\right]_x - \left[(\partial_{k_x}\mathbf{d})\times\mathbf{d}\right]_y\right\}\left[\theta\left(|\mu|-|\mathbf{d}|\right) + |\mathbf{d}|\delta\left(|\mu|-|\mathbf{d}|\right)\right], \tag{26}$$

as well as the following spatial components of the chiral current density:

$$J_n^5 = -\frac{e^2 B_5 a \Lambda}{2\sin(ab_z)} \int \frac{d^3\mathbf{k}}{(2\pi)^3} \sin(ak_z)\,\mathrm{sgn}(\mu)\,\delta\left(\mu^2 - |\mathbf{d}|^2\right)\,\chi(\mathbf{k})\,\Big\{\left[(\partial_{k_n}\mathbf{d})\times(\partial_{k_y}\mathbf{d})\right]_x - \left[(\partial_{k_n}\mathbf{d})\times(\partial_{k_x}\mathbf{d})\right]_y\Big\}. \quad (27)$$

We found that after the integration over the Brillouin zone the chiral current density vanishes, i.e., $\mathbf{J}^5 = 0$.

Since the vacuum part of the chiral charge density (25) is the most interesting from the topological viewpoint, we will analyse below only this contribution by setting $\mu = 0$. Integrating over the Brillouin zone in Eq. (25), we find numerically that the chiral charge density ρ_0^5 is nonzero. This result together with $\mathbf{J}^5 = 0$ qualitatively agrees with the expected response. Indeed, as we mentioned in the Introduction, the chiral counterpart of the BZCS term could be established in the relativistic field theory by using the arguments of the consistent anomaly [39, 40] and equals $j^\nu_{5,\,\mathrm{BZCS}} = -e^2\epsilon^{\nu\rho\alpha\beta}A^5_\rho F^5_{\alpha\beta}/(12\pi^2)$. In a background pseudomagnetic field, the latter gives a nonzero contribution to the chiral charge density

$$\rho^5_{\mathrm{BZCS}} = -\frac{e^2 B_5 b_z}{6\pi^2}. \quad (28)$$

An analysis of the expression in Eq. (25) reveals, however, that the actual chiral charge density in the lattice model at hand differs from the expected BZCS result in Eq. (28). While the inability to reproduce the BZCS may seem surprising, this might have been expected for the chirality implemented on the lattice. Moreover, since the chirality is not well defined away from the Weyl nodes in the lattice model, one may even expect that the deviations from the default BZCS result $j^\nu_{5,\,\mathrm{BZCS}}$ depends on the actual definition of chirality. We also find that another source of the deviations is related to the nature of the pseudoelectromagnetic fields, which are not coupled minimally in the whole Brillouin zone.

The numerical results for the relative difference of the chiral charge densities $\Delta\rho^5/\rho^5_{\mathrm{BZCS}} = (\rho^5_{\mathrm{BZCS}} - \rho^5_0)/\rho^5_{\mathrm{BZCS}}$ are plotted in Fig. 3 as a function of ϵ_0. As is clear from the results presented, the deviations from the BZCS chiral charge density are substantial and model dependent. Also, neither definition of the chirality reproduces Eq. (28) exactly. We conclude, therefore, that the chiral BZCS term $j^\nu_{5,\,\mathrm{BZCS}}$, unlike its electric counterpart, is not topologically protected in the lattice models of Weyl materials.

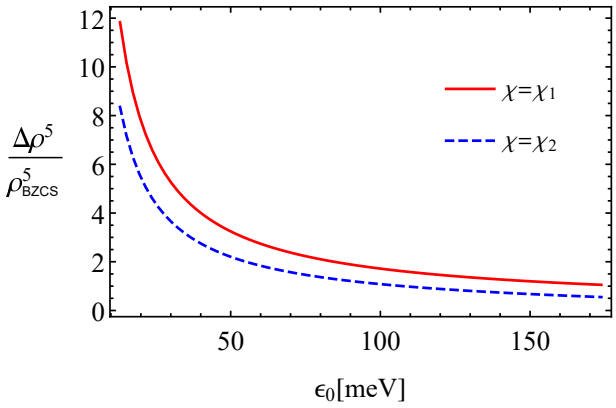

FIG. 3. The dependence of the relative difference of the chiral charge density $\Delta\rho^5/\rho^5_{\mathrm{BZCS}} = (\rho^5_{\mathrm{BZCS}} - \rho^5_0)/\rho^5_{\mathrm{BZCS}}$ on ϵ_0 for the two definitions of chirality: $\chi(\mathbf{k}) = \chi_1(\mathbf{k})$ (red solid line) and $\chi(\mathbf{k}) = \chi_2(\mathbf{k})$ (dashed blue line). The results are plotted for the model parameters given in Appendix A and the vanishing chemical potential $\mu = 0$.

Finally, it is instructive to discuss the physical meaning of the chiral charge density ρ^5 induced by the pseudomagnetic field. The vacuum and matter contributions given in Eqs. (25) and (26), respectively, break parity and, therefore, effectively create an optically active medium. The value of ρ^5 is the quantitative measure of the optical activity and, thus, can be observed via polarized optical probes similar to those used in studies of transition metal dichalcogenides [55, 56].

B. Response to a pseudoelectric field

Similarly to the study of the response to a background electric field in Sec. IV, we derive the following formal expression for the generalized chiral DC conductivity tensor:

$$\sigma^{5,5}_{\nu m,\mathrm{tot}} = \lim_{\Omega\to 0}\frac{i}{\Omega}T\sum_{l=-\infty}^{\infty}\int\frac{d^3\mathbf{k}}{(2\pi)^3}\int\int d\omega d\omega'\,\frac{\chi(\mathbf{k})\,\mathrm{tr}\left[j_\nu(\mathbf{k})A(\omega;\mathbf{k})j^5_m(\mathbf{k})A(\omega';\mathbf{k})\right]}{(i\omega_l+\mu-\omega)\,(i\omega_l-\Omega-i0+\mu-\omega')} \tag{29}$$

which defines the response of the chiral charge and current densities to a pseudoelectric field $\mathbf{E}_5$. After performing the summation over the Matsubara frequencies and setting $T=0$ afterwards, we derive the following result for the generalized chiral conductivity tensor:

$$\sigma^{5,5}_{0m} = -e^2\pi\int\frac{d^3\mathbf{k}}{(2\pi)^3}\chi(\mathbf{k})\,\frac{\delta^2_\Gamma(\mu-|\mathbf{d}|)-\delta^2_\Gamma(\mu+|\mathbf{d}|)}{|\mathbf{d}|}d_m\tilde{j}^5_m, \tag{30}$$

$$\tilde{\sigma}^{5,5}_{nm} = e\int\frac{d^3\mathbf{k}}{(2\pi)^3}\frac{\chi(\mathbf{k})\,\tilde{j}^5_m\,[\mathbf{d}\times(\partial_{k_n}\mathbf{d})]_m}{2|\mathbf{d}|^3}\left[1-\theta(|\mu|-|\mathbf{d}|)\right], \tag{31}$$

$$\sigma^{5,5}_{nm} = -2e^2\pi\int\frac{d^3\mathbf{k}}{(2\pi)^3}\frac{\chi(\mathbf{k})}{4|\mathbf{d}|^2}\sum_{s,s'=\pm}\delta_\Gamma(\mu-s|\mathbf{d}|)\delta_\Gamma(\mu-s'|\mathbf{d}|)\Big\{|\mathbf{d}|^2\,(\partial_{k_n}d_m)\,\tilde{j}^5_m$$
$$+\,2ss'\,((\partial_{k_n}\mathbf{d})\cdot\mathbf{d})\,\tilde{j}^5_m d_m - ss'(\partial_{k_n}d_m)\tilde{j}^5_m|\mathbf{d}|^2\Big\}, \tag{32}$$

where $\tilde{j}^5_n=\sum_{m=1}^3\mathrm{tr}\left(\sigma_n j^5_m\right)/2$ and we also separated the nondissipative $\tilde{\sigma}^{5,5}_{nm}$ and dissipative $\sigma^{5,5}_{nm}$ parts of the tensor. Our direct numerical calculations show that, unlike the response to electric field $\mathbf{E}$, there are nontrivial diagonal components of the generalized chiral conductivity tensor, $\sigma^{5,5}_{11}=\sigma^{5,5}_{22}$, and $\sigma^{5,5}_{33}$, as well as the off-diagonal components $\tilde{\sigma}^{5,5}_{12}=-\tilde{\sigma}^{5,5}_{21}$, which describe the chiral analog of the anomalous Hall effect. The corresponding numerical results for the diagonal components are presented in Fig. 4. The dissipative parts $\sigma^{5,5}_{11}$ and $\sigma^{5,5}_{33}$ are almost insensitive to the definition of chirality, therefore, we present the results only for $\chi(\mathbf{k})=\chi_2(\mathbf{k})$. Further, it is important to note that while the dependence of $\sigma^{5,5}_{11}$ on μ is monotonous and demonstrates only a slight change at $|\mu|=\epsilon_0$, this is not the case for $\sigma^{5,5}_{33}$. The latter shows an upturn at $|\mu|\approx\epsilon_0$, which is clearly pronounced at small values of Γ_0. We can explain this fact by noting that the chirality $\chi(\mathbf{k})$ becomes ill-defined in the vicinity of the Lifshitz transition, when the two chiral Fermi sheets or, equivalently, valleys overlap. Finally, both conductivities show the steep increase at small values of μ.

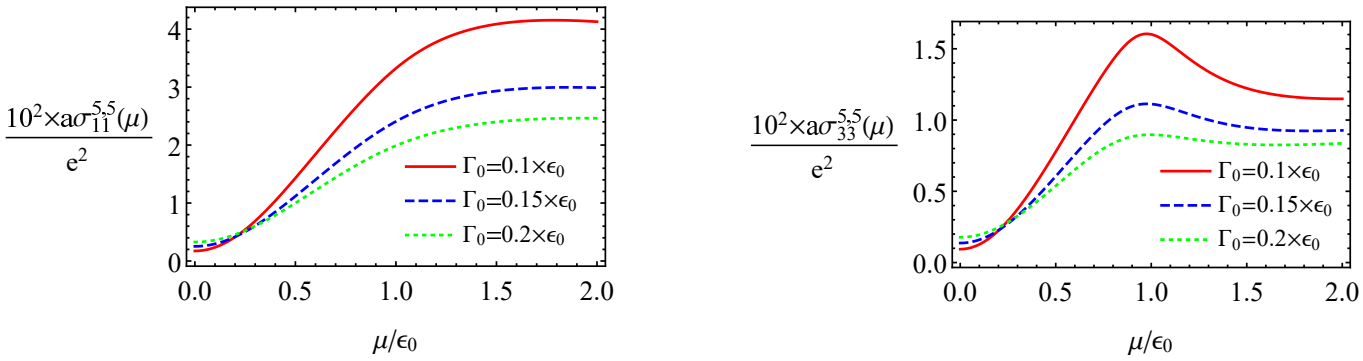

FIG. 4. The dependence of the diagonal components of the generalized chiral conductivity tensor on the chemical potential: $\sigma^{5,5}_{11}$ (left panel), and $\sigma^{5,5}_{33}$ (right panel). The red solid, blue dashed, and green dotted lines correspond to $\Gamma_0=0.1\,\epsilon_0$, $\Gamma_0=0.15\,\epsilon_0$, and $\Gamma_0=0.2\,\epsilon_0$, respectively. The results are plotted for the model parameters given in Appendix A.

The nondissipative part in Eq. (31) looks like a quantity of the topological origin and is comparable to the expression of the chiral anomalous Hall effect suggested in Refs. [39, 40] in the framework of the consistent anomaly, i.e.,

$$\sigma_{5,\mathrm{AHE}} = -\frac{e^2 b_z}{6\pi^2}. \tag{33}$$

However, a closer examination reveals that even the off-diagonal component $\tilde{\sigma}_{12}^{5,5}$ in Eq. (31), describing the anomalous chiral Hall effect, is model dependent and, thus, is not fixed unambiguously by topology alone. Independent of the details, though, it is interesting to note that the anomalous chiral Hall effect vanishes in the limit of large chemical potential, as is evident from Eq. (31) where $\theta(|\mu| - |\mathbf{d}|) \to 1$. Of course, this result is not surprising in a lattice model with a finite width of the energy band. Moreover, we also found that all chiral response coefficients vanish in the limit of large μ. (This may not always appear evident from the numerical results in this study because we concentrate primarily on the energy region near the Weyl nodes.)

The absence of topological robustness in the anomalous part $\tilde{\sigma}_{12}^{5,5}$ is clear from Fig. 5, where we present the dependence of $\tilde{\sigma}_{12}^{5,5}/\sigma_{5,\mathrm{AHE}}$ on the chemical potential. The two definitions of chirality give the results that are almost a factor of 3 different from each other, although otherwise have a qualitatively similar dependence on μ. Interestingly, while there is only a small quantitative discrepancy between the $\tilde{\sigma}_{12}^{5,5}$ at $\chi(\mathbf{k}) = \chi_1(\mathbf{k})$ and $\sigma_{5,\mathrm{AHE}}$ for a given set of parameters, neither of the definitions [as well as the linearized model result (33) of Refs. [39, 40]] quantitatively agrees with the result in Ref. [71]. In addition to the problem with the definition of chirality far from the Weyl nodes, we attribute this difference also to the fact that strains in Weyl materials can be described in terms of pseudoelectromagnetic fields only near the Weyl nodes. Note that the "material" part of the response, e.g., electric current in strain-induced pseudomagnetic field studied in Ref. [44], agrees with its linearized value at small μ because it is determined only by the states in the vicinity of the nodes.

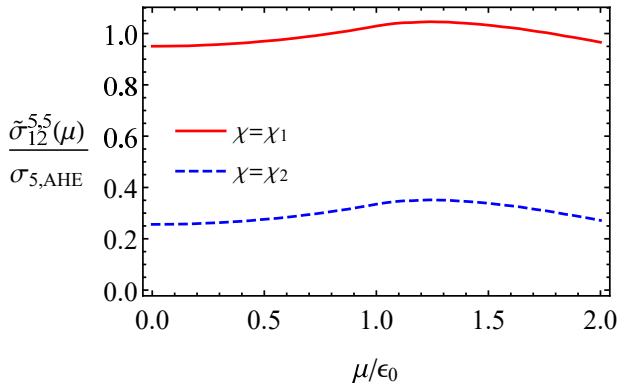

FIG. 5. The dependence of the off-diagonal component of the generalized chiral conductivity tensor $\tilde{\sigma}_{12}^{5,5}$ on the chemical potential, normalized by $\sigma_{5,\mathrm{AHE}} = -e^2 b_z/(6\pi^2)$. The results are plotted for the model parameters given in Appendix A.

VI. SUMMARY AND DISCUSSIONS

In this paper we investigated the response of the chiral (valley) charge and current densities to background electromagnetic and pseudoelectromagnetic fields in a lattice model of Weyl materials. By comparing the results with those for the electric charge and current densities obtained in the same lattice model [44], our main finding is that the chiral counterpart of the BZCS current is not topologically robust. In essence, the key to understanding the distinction between the results for these two sets of observables lies in the profound difference between the definitions of the exactly conserved electric charge and a less unambiguous concept of chirality on the lattice. In a common sense, the latter is well defined only in a close vicinity of the Weyl nodes.

These conclusions are supported by the direct calculations of the chiral charge density induced by a pseudomagnetic field as well as the anomalous chiral Hall effect in a pseudoelectric field. By studying the response to strain-induced pseudoelectromagnetic fields, we found that the "vacuum" contributions to chiral charge and current densities (i.e., the contributions independent of the chemical potential and disorder) deviate considerably from those given by the BZCS expression obtained in relativistic field theory by using the arguments of the consistent anomaly [39, 40]. Our calculations show that the chiral charge induced by the pseudomagnetic field and the corresponding conductivity of the anomalous chiral Hall effect in a background pseudoelectric field depend on the definition of chirality and the parameters of the model. This is in drastic contrast to the truly topological BZCS terms of the electric charge and current densities studied in Refs. [22–27, 32, 33, 44]. We conclude, therefore, that the chiral analogs of the BZCS terms in Weyl materials have a very different nontopological status. We believe that the absence of the topological protection of the chiral counterpart of the BZCS current is related also to the fact that strains can be interpreted as pseudoelectromagnetic fields only in the vicinity of Weyl nodes. However, this does not diminish by any means the

potential practical value of the chiral (or valley) transport in Weyl materials. Indeed, even a nontopological anomalous chiral Hall effect could find useful applications that rely on the chirality (or valley) degrees of freedom.

We analysed also the chiral separation effect in the lattice model. As anticipated, it is reproduced nearly exactly at small values of the chemical potential μ. At large values of μ, on the other hand, we found that the chiral current density deviates considerably from its counterpart in the linearized model. This is easy to understand by noting that the system undergoes a Lifshitz transition when the chemical potential is equal to ϵ_0. As a result, in the regime with $|\mu| > \epsilon_0$, the Fermi surfaces for the opposite chirality Weyl quasiparticles are not even separated from each other. Therefore, it is quite natural that the chiral current diminishes considerably for $|\mu| > \epsilon_0$. As expected, we found that in general the chiral responses vanish at large values of chemical potential $|\mu| \gg \epsilon_0$ because the Brillouin zone becomes completely filled and quasiparticles are no longer described by the Weyl equation. We would like to note also that the results for the chiral response in electromagnetic fields can be applied for the simulation of truly relativistic Weyl plasma with a lattice regularization.

Finally, we would like to discuss how the chiral response in Weyl materials could be experimentally probed. Unlike the electric current, the chiral one is not directly experimentally observable. Nevertheless, an interplay between the electric and chiral currents produces new types of collective excitations (e.g., the chiral magnetic waves and chiral plasmons) which can reveal indirectly the chiral response. On the other hand, a response in the form of a nonzero chiral charge density ρ^5 effectively creates an optically active medium. Thus, it can be investigated via polarized optical probes.

ACKNOWLEDGMENTS

The work of E.V.G. was partially supported by the Program of Fundamental Research of the Physics and Astronomy Division of the National Academy of Sciences of Ukraine. The work of V.A.M. and P.O.S. was supported by the Natural Sciences and Engineering Research Council of Canada. The work of I.A.S. was supported by the U.S. National Science Foundation under Grants PHY-1404232 and PHY-1713950.

Appendix A: Model details

In this appendix we give the details of the lattice model used in the main text of the paper. The functions d_0 and $\mathbf{d}$ have the following dependence on the components of the momentum:

$$d_0 = g_0 + g_1 \cos(a_z k_z) + g_2 \left[\cos(a_x k_x) + \cos(a_y k_y)\right], \tag{A1}$$
$$d_1 = \Lambda \sin(a_x k_x), \tag{A2}$$
$$d_2 = \Lambda \sin(a_y k_y), \tag{A3}$$
$$d_3 = t_0 + t_1 \cos(a_z k_z) + t_2 \left[\cos(a_x k_x) + \cos(a_y k_y)\right], \tag{A4}$$

where a_x, a_y, and a_z denote the lattice spacings. As in Ref. [44], we choose the model parameters by using the parametrization for Na_3Bi [12],

$$t_0 = M_0 - t_1 - 2t_2, \quad t_{1,2} = -\frac{2M_{1,2}}{a^2}, \tag{A5}$$
$$g_0 = C_0 - g_1 - 2g_2, \quad g_{1,2} = -\frac{2C_{1,2}}{a^2}, \tag{A6}$$
$$\Lambda = \frac{A}{a}, \tag{A7}$$

where

$$\begin{array}{lll} C_0 = -0.06382 \text{ eV}, & C_1 = 8.7536 \text{ eV Å}^2, & C_2 = -8.4008 \text{ eV Å}^2, \\ M_0 = 0.08686 \text{ eV}, & M_1 = -10.6424 \text{ eV Å}^2, & M_2 = -10.3610 \text{ eV Å}^2, \\ A = 2.4598 \text{ eV Å}. & & \end{array} \tag{A8}$$

Also, for simplicity, we assumed that the lattice is cubic, i.e., $a_x = a_y = a_z = a \approx 7.5$ Å.

The dispersion relations of (quasi)particles described by Hamiltonian (1) are given by

$$\epsilon_{\mathbf{k}} = d_0 \pm |\mathbf{d}|. \tag{A9}$$

By making use of Eqs. (A1)–(A4), it is straightforward to show that the lattice model has two Weyl nodes if $|t_0+2t_2| \leq |t_1|$. The corresponding chiral shift parameter b_z is given by the following expression:

$$b_z = \frac{1}{a}\arccos\left(\frac{-t_0-2t_2}{t_1}\right). \tag{A10}$$

The energy spectrum of the model is shown in Fig. 6 for several values of parameters t_1. As is clear, the value of t_1 affects the momentum space separation between the Weyl nodes and the value of the Fermi velocity. Note that the energy in Fig. 6 is shown in units of $\epsilon_0 = \lim_{\mathbf{k}\to\mathbf{0}}|\mathbf{d}|$. This characteristic value of energy represents the height of the "dome" between the Weyl nodes.

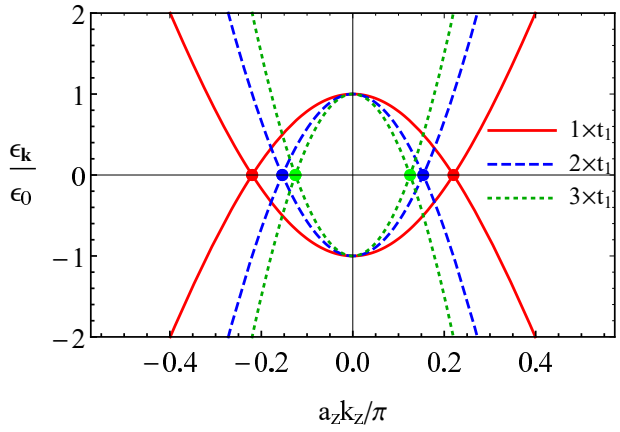

FIG. 6. The energy spectrum (A9) at $d_0 = 0$ for several different values of t_1 at $k_x = k_y = 0$.

By starting from the model Hamiltonian (1), at the zeroth order in external electromagnetic fields, it is straightforward to derive the Green's function (Feynman propagator) in reciprocal space

$$G^{(0)}(\omega;\mathbf{k}) = \frac{i\left[\omega+\mu+(\mathbf{d}\cdot\boldsymbol{\sigma})\right]}{\left[\omega+\mu+i0\,\mathrm{sgn}\,(\omega)\right]^2-|\mathbf{d}|^2}, \tag{A11}$$

where μ is the chemical potential. The corresponding spectral function is given by

$$A(\omega;\mathbf{k}) \equiv \frac{i}{2\pi}\left[G^{(0)}(\omega+i0;\mathbf{k})-G^{(0)}(\omega-i0;\mathbf{k})\right]_{\mu=0} = i\sum_{s=\pm}\frac{|\mathbf{d}|+s(\mathbf{d}\cdot\boldsymbol{\sigma})}{2|\mathbf{d}|}\delta\left(\omega-s|\mathbf{d}|\right), \tag{A12}$$

where, in order to model phenomenologically a nonzero transport quasiparticle width Γ, we replaced the δ-function in the last representation with the Lorentzian distribution

$$\delta_\Gamma(\omega-s|\mathbf{d}|) \equiv \frac{1}{\pi}\frac{\Gamma(\omega)}{(\omega-s|\mathbf{d}|)^2+\Gamma^2(\omega)}. \tag{A13}$$

We will assume that the transport quasiparticle width includes a constant, as well as a frequency-dependent part proportional to ω^2 [70], i.e., $\Gamma(\omega) = \Gamma_0(1+\omega^2/\epsilon_0^2)$.

Appendix B: Chiral charge and current densities in background magnetic and electric fields

In this appendix we outline briefly the derivation of the chiral charge and current densities in background magnetic and electric fields. It might be instructive to start by recalling the expressions for the electric charge and current densities [44]

$$\rho = -e\lim_{r'\to r}\mathrm{tr}\left[G(r,r')\right], \tag{B1}$$

$$\mathbf{J} = -\lim_{r'\to r}\mathrm{tr}\left[\mathbf{j}(-i\boldsymbol{\nabla}_\mathbf{r})G(r,r')\right], \tag{B2}$$

where $G(r,r')$ is the (quasi)particles Green's function, $r=(t,\mathbf{r})$, $r'=(t',\mathbf{r}')$, and the electric current density operator in the momentum space is given by

$$\mathbf{j}(\mathbf{k}) = -e\boldsymbol{\nabla}_{\mathbf{k}}\mathcal{H}_{\rm latt}. \tag{B3}$$

The chiral analogs of the quantities in Eqs. (B1) and (B2) are similar, but contain an additional insertion of the chirality operator $\chi(\mathbf{k})$ under the trace. In order to calculate the chiral charge and current densities in the first order in the background electromagnetic field, we need to determine the corresponding first-order correction to the Green's function $G^{(1)}(r,r')$, i.e.,

$$G^{(1)}(r,r') = -i\int dr'' G^{(0)}(r-r'')\left(\mathbf{A}(r'')\cdot\mathbf{j}(-i\boldsymbol{\nabla}_{\mathbf{r}''})\right)G^{(0)}(r''-r'). \tag{B4}$$

By using the same approach as in Appendix C of Ref. [44], we then derive the chiral charge and current densities in the following form:

$$\rho^5 = \frac{eB}{2}\int\frac{d\omega d^3\mathbf{k}}{(2\pi)^4}\chi(\mathbf{k})\,\mathrm{tr}\Big\{\left[\partial_{k_x}G^{(0)}(\omega,\mathbf{k})\right]j_y(\mathbf{k})G^{(0)}(\omega,\mathbf{k}) - G^{(0)}(\omega,\mathbf{k})j_y(\mathbf{k})\left[\partial_{k_x}G^{(0)}(\omega,\mathbf{k})\right]\Big\}, \tag{B5}$$

$$\begin{aligned} J^5_n = \frac{B}{2}\int\frac{d\omega d^3\mathbf{k}}{(2\pi)^4}\chi(\mathbf{k})\,\mathrm{tr}\Big\{&j_n(\mathbf{k})\left[\partial_{k_x}G^{(0)}(\omega,\mathbf{k})\right]j_y(\mathbf{k})G^{(0)}(\omega,\mathbf{k}) - j_n(\mathbf{k})G^{(0)}(\omega,\mathbf{k})j_y(\mathbf{k})\left[\partial_{k_x}G^{(0)}(\omega,\mathbf{k})\right]\\ &+\delta_{n,x}\left[\partial_{k_x}j_x(\mathbf{k})\right]G^{(0)}(\omega,\mathbf{k})j_y(\mathbf{k})G^{(0)}(\omega,\mathbf{k}) + 2ir_n\delta_{n,x}G^{(0)}(\omega,\mathbf{k})j_y(\mathbf{k})G^{(0)}(\omega,\mathbf{k})\Big\}. \end{aligned} \tag{B6}$$

In the derivation, we used the linear-order correction to the Green's function in Eq. (B4), as well as the definitions for the chiral charge and current densities analogous to those in Eqs. (B1) and (B2), but with the additional insertion of the chirality operator $\chi(\mathbf{k})$ defined by either Eq. (6) or Eq. (7).

By taking into account that the definitions in Eqs. (B5) and (B6) differ from the corresponding expressions for the electric charge and current densities in Ref. [44] only by the insertion of the chirality operator $\chi(\mathbf{k})$, the final results for the chiral or valley polarization and current densities can be written down without repeating the intermediate steps of derivation.

1. Background magnetic field

Similarly to the results in Appendix E 1 in Ref. [44], the final expression for the chiral charge density in a background magnetic field is given by

$$\rho^5 = eB\int\frac{d\omega d\mathbf{k}}{(2\pi)^4}\chi(\mathbf{k})\sum_{i_1,i_2,i_3=1}^{3}\frac{2i\epsilon_{i_1i_2i_3}\left(\partial_{k_x}d_{i_1}\right)\left(\partial_{k_y}d_{i_2}\right)d_{i_3}}{\left[(\omega+\mu-\epsilon_0+i0\,\mathrm{sgn}\,(\omega))^2-\mathbf{d}^2\right]^2}. \tag{B7}$$

After the integration over ω, the result contains two parts given in Eqs. (8) and (13) in the main text.

The final expression for the chiral current density is given by

$$J^5_n = -e^2B\int\frac{d\mathbf{k}}{(2\pi)^3}\chi(\mathbf{k})\;\mathrm{sgn}\,(\mu)\sum_{i_1,i_2,i_3=1}^{3}\epsilon_{i_1i_2i_3}(\partial_{k_n}d_{i_1})(\partial_{k_x}d_{i_2})(\partial_{k_y}d_{i_3})\delta\left(\mu^2-|\mathbf{d}|^2\right), \tag{B8}$$

where the integration over ω was already performed. Note that we also dropped several (imaginary) terms that vanished after the integration over the Brillouin zone.

2. Background electric field

By making use of the results in Appendix E of Ref. [44], we can also write down the expression for the chiral version of the generalized conductivity tensor. The corresponding result simply has the additional chirality insertion.

In particular,

$$\sigma_{0m} = e^2\pi\int\frac{d^3\mathbf{k}}{(2\pi)^3}\int d\omega\frac{1}{4T\cosh^2\left(\frac{\omega-\mu}{2T}\right)}\frac{\chi(\mathbf{k})}{2|\mathbf{d}|}\sum_{s,s'=\pm}ss'\delta_\Gamma(\omega-s|\mathbf{d}|)\delta_\Gamma(\omega-s'|\mathbf{d}|)(s+s')\left(\mathbf{d}\cdot(\partial_{k_m}\mathbf{d})\right)$$
$$\overset{T\to0}{=} e^2\pi\int\frac{d^3\mathbf{k}}{(2\pi)^3}\chi(\mathbf{k})\frac{\delta_\Gamma^2(\mu-|\mathbf{d}|)-\delta_\Gamma^2(\mu+|\mathbf{d}|)}{|\mathbf{d}|}\left(\mathbf{d}\cdot(\partial_{k_m}\mathbf{d})\right). \tag{B9}$$

For spatial components of the tensor, the result can be written in the form of two contributions

$$\sigma^5_{nm} = \sigma^{5,(1)}_{nm} + \sigma^{5,(2)}_{nm}, \tag{B10}$$

where

$$\sigma^{5,(1)}_{nm} = -e^2\lim_{\Omega\to0}\frac{1}{\Omega}\int\frac{d^3\mathbf{k}}{(2\pi)^3}\int\int d\omega d\omega'\frac{n_F(\omega)-n_F(\omega')}{\omega-\omega'-\Omega}\frac{1}{4|\mathbf{d}|^2}\sum_{s,s'=\pm}ss'\delta_\Gamma(\omega-s|\mathbf{d}|)\delta_\Gamma(\omega'-s'|\mathbf{d}|)$$
$$\times\,2\chi(\mathbf{k})\sum_{i_1,i_2,i_3=1}^{3}\epsilon_{i_1i_2i_3}(\partial_{k_n}d_{i_1})d_{i_2}(\partial_{k_m}d_{i_3}), \tag{B11}$$

and

$$\sigma^{5,(2)}_{nm} = e^2\pi\int\frac{d\mathbf{k}}{(2\pi)^3}\int d\omega\frac{\chi(\mathbf{k})}{2T\cosh^2\left(\frac{\omega-\mu}{2T}\right)}\frac{1}{4|\mathbf{d}|}\sum_{s,s'=\pm}ss'\delta_\Gamma(\omega-s|\mathbf{d}|)\delta_\Gamma(\omega'-s'|\mathbf{d}|)\Big[ss'|\mathbf{d}|^2\left((\partial_{k_n}\mathbf{d})\cdot(\partial_{k_m}\mathbf{d})\right)$$
$$+\sum_{i_1,i_2,i_3,i_4=1}^{3}\left(\delta_{i_1i_2}\delta_{i_3i_4}-\delta_{i_1i_3}\delta_{i_2i_4}+\delta_{i_1i_4}\delta_{i_2i_3}\right)(\partial_{k_n}d_{i_1})d_{i_2}(\partial_{k_m}d_{i_3})d_{i_4}\Big]. \tag{B12}$$

The first term in the chiral conductivity tensor $\sigma^{5,(1)}_{nm}$ can be written in much simpler form in the clean limit $\Gamma\to0$

$$\sigma^{5,(1)}_{nm} = e^2\int\frac{d\mathbf{k}}{(2\pi)^3}\frac{\chi(\mathbf{k})}{2|\mathbf{d}|^3}\left[n_F(-|\mathbf{d}|)-n_F(|\mathbf{d}|)\right]\sum_{i_1,i_2,i_3=1}^{3}\epsilon_{i_1i_2i_3}(\partial_{k_n}d_{i_1})d_{i_2}(\partial_{k_m}d_{i_3}), \tag{B13}$$

where the integration over ω was performed. Note that $n_F(\omega)=1/\left[e^{(\omega-\mu)/T}+1\right]$ is the Fermi-Dirac distribution. As is easy to check, in the zero temperature limit, this reduces to the result in Eq. (18) in the main text. The result in Eq. (19) comes from $\sigma^{5,(2)}_{nm}$ in the limit $T\to0$ after the integration over ω is performed.

[1] X. Wan, A. M. Turner, A. Vishwanath, and S. Y. Savrasov, Phys. Rev. B **83**, 205101 (2011).
[2] H. M. Weng, C. Fang, Z. Fang, B. A. Bernevig, and X. Dai, Phys. Rev. X **5**, 011029 (2015).
[3] B. Q. Lv, H. M. Weng, B. B. Fu, X. P. Wang, H. Miao, J. Ma, P. Richard, X. C. Huang, L. X. Zhao, G. F. Chen, Z. Fang, X. Dai, T. Qian, and H. Ding, Phys. Rev. X **5**, 031013 (2015).
[4] X. Huang, L. Zhao, Y. Long, P. Wang, D. Chen, Z. Yang, H. Liang, M. Xue, H. Weng, Z. Fang, X. Dai, and G. Chen, Phys. Rev. X **5**, 031023 (2015).
[5] S.-Y. Xu, I. Belopolski, N. Alidoust, M. Neupane, G. Bian, C. Zhang, R. Sankar, G. Chang, Z. Yuan, C.-C. Lee, S.-M. Huang, H. Zheng, J. Ma, D. S. Sanchez, B. Wang, A. Bansil, F. Chou, P. P. Shibayev, H. Lin, S. Jia, and M. Z. Hasan, Science **349**, 613 (2015).
[6] S.-M. Huang, S.-Y. Xu, I. Belopolski, C.-C. Lee, G. Chang, B. Wang, N. Alidoust, G. Bian, M. Neupane, C. Zhang, S. Jia, A. Bansil, H. Lin, and M. Z. Hasan Nat. Commun. **6**, 7373 (2015).
[7] C.-L. Zhang, S.-Y. Xu, I. Belopolski, Z. Yuan, Z. Lin, B. Tong, G. Bian, N. Alidoust, C.-C. Lee, S.-M. Huang, T.-R. Chang, G. Chang, C.-H. Hsu, H.-T. Jeng, M. Neupane, D. S. Sanchez, H. Zheng, J. Wang, H. Lin, C. Zhang, H.-Z. Lu, S.-Q. Shen, T. Neupert, M. Z. Hasan, and S. Jia, Nat. Commun. **7**, 10735 (2016).
[8] S. Borisenko, D. Evtushinsky, Q. Gibson, A. Yaresko, T. Kim, M. N. Ali, B. Buechner, M. Hoesch, and R. J. Cava, arXiv:1507.04847.
[9] I. Belopolski, S.-Y. Xu, Y. Ishida, X. Pan, P. Yu, D. S. Sanchez, M. Neupane, N. Alidoust, G. Chang, T.-R. Chang, Y. Wu, G. Bian, H. Zheng, S.-M. Huang, C.-C. Lee, D. Mou, L. Huang, Y. Song, B. Wang, G. Wang, Y.-W. Yeh, N. Yao, J. Rault, P. Lefevre, F. Bertran, H.-T. Jeng, T. Kondo, A. Kaminski, H. Lin, Z. Liu, F. Song, S. Shin, and M. Z. Hasan, arXiv:1512.09099.
[10] H. B. Nielsen and M. Ninomiya, Nucl. Phys. B **185**, 20 (1981); **195**, 541 (1982); **193**, 173 (1981).

[11] Z. Wang, H. Weng, Q. Wu, X. Dai, and Z. Fang, Phys. Rev. B **88**, 125427 (2013).
[12] Z. Wang, Y. Sun, X. Q. Chen, C. Franchini, G. Xu, H. Weng, X. Dai, and Z. Fang, Phys. Rev. B **85**, 195320 (2012).
[13] H. Weng, X. Dai, and Z. Fang, Phys. Rev. X **4**, 011002 (2014).
[14] S. Borisenko, Q. Gibson, D. Evtushinsky, V. Zabolotnyy, B. Buchner, and R. J. Cava, Phys. Rev. Lett. **113**, 027603 (2014).
[15] M. Neupane, S.-Y. Xu, R. Sankar, N. Alidoust, G. Bian, C. Liu, I. Belopolski, T.-R. Chang, H.-T. Jeng, H. Lin, A. Bansil, F. Chou, and M. Z. Hasan, Nature Commun. **5**, 3786 (2014).
[16] Z. K. Liu, B. Zhou, Y. Zhang, Z. J. Wang, H. M. Weng, D. Prabhakaran, S.-K. Mo, Z. X. Shen, Z. Fang, X. Dai, Z. Hussain, and Y. L. Chen, Science **343**, 864 (2014).
[17] J. Xiong, S. K. Kushwaha, T. Liang, J. W. Krizan, M. Hirschberger, W. Wang, R. J. Cava, and N. P. Ong, Science **350**, 413 (2015).
[18] C.-Z. Li, L.-X. Wang, H. Liu, J. Wang, Z.-M. Liao, and D.-P. Yu, Nat. Commun. **6**, 10137 (2015).
[19] H. Li, H. He, H.-Z. Lu, H. Zhang, H. Liu, R. Ma, Z. Fan, S.-Q. Shen, and J. Wang, Nat. Commun. **7**, 10301 (2016).
[20] Q. Li, D. E. Kharzeev, C. Zhang, Y. Huang, I. Pletikosic, A. V. Fedorov, R. D. Zhong, J. A. Schneeloch, G. D. Gu, and T. Valla, Nature Phys. **12**, 550 (2016).
[21] M. V. Berry, Proc. R. Soc. A **392**, 45 (1984).
[22] K.-Y. Yang, Y.-M. Lu, and Y. Ran, Phys. Rev. B **84**, 075129 (2011).
[23] A. A. Burkov and L. Balents, Phys. Rev. Lett. **107**, 127205 (2011).
[24] A. A. Burkov, Phys. Rev. Lett. **113**, 187202 (2014).
[25] A. G. Grushin, Phys. Rev. D **86**, 045001 (2012).
[26] A. A. Zyuzin and A. A. Burkov, Phys. Rev. B **86**, 115133 (2012).
[27] P. Goswami and S. Tewari, Phys. Rev. B **88**, 245107 (2013).
[28] V. Aji, Phys. Rev. B **85**, 241101 (2012).
[29] D. T. Son and B. Z. Spivak, Phys. Rev. B **88**, 104412 (2013).
[30] E. V. Gorbar, V. A. Miransky, and I. A. Shovkovy, Phys. Rev. B **89**, 085126 (2014).
[31] A. A. Burkov, Phys. Rev. B **91**, 245157 (2015).
[32] M. M. Vazifeh and M. Franz, Phys. Rev. Lett. **111**, 027201 (2013).
[33] G. Basar, D. E. Kharzeev, and H. U. Yee, Phys. Rev. B **89**, 035142 (2014).
[34] K. Fukushima, D. E. Kharzeev, and H. J. Warringa, Phys. Rev. D **78**, 074033 (2008).
[35] D. T. Son and N. Yamamoto, Phys. Rev. Lett. **109**, 181602 (2012).
[36] M. A. Stephanov and Y. Yin, Phys. Rev. Lett. **109**, 162001 (2012).
[37] D. T. Son and N. Yamamoto, Phys. Rev. D **87**, 085016 (2013).
[38] S. L. Adler, Phys. Rev. **177**, 2426 (1969); J. S. Bell and R. Jackiw, Nuovo Cim. A **60**, 47 (1969).
[39] K. Landsteiner, Phys. Rev. B **89**, 075124 (2014).
[40] K. Landsteiner, Acta Phys. Polonica B **47**, 2617 (2016).
[41] E. V. Gorbar, V. A. Miransky, I. A. Shovkovy, and P. O. Sukhachov, Phys. Rev. Lett. **118**, 127601 (2017).
[42] E. V. Gorbar, V. A. Miransky, I. A. Shovkovy, and P. O. Sukhachov, Phys. Rev. B **95**, 115202 (2017); 115422 (2017).
[43] W. A. Bardeen, Phys. Rev. **184**, 1848 (1969); W. A. Bardeen and B. Zumino, Nucl. Phys. B **244**, 421 (1984).
[44] E. V. Gorbar, V. A. Miransky, I. A. Shovkovy, and P. O. Sukhachov, Phys. Rev. B **96**, 085130 (2017).
[45] J. Zhou, H. Jiang, Q. Niu, and J. Shi, Chin. Phys. Lett. **30**, 027101 (2013).
[46] M. A. Zubkov, Annals Phys. **360**, 655 (2015).
[47] A. Cortijo, Y. Ferreiros, K. Landsteiner, and M. A. H. Vozmediano, Phys. Rev. Lett. **115**, 177202 (2015).
[48] A. Cortijo, D. Kharzeev, K. Landsteiner, and M. A. H. Vozmediano, Phys. Rev. B **94**, 241405 (2016)
[49] A. G. Grushin, J. W. F. Venderbos, A. Vishwanath, and R. Ilan, Phys. Rev. X **6**, 041046 (2016).
[50] D. I. Pikulin, A. Chen, and M. Franz, Phys. Rev. X **6**, 041021 (2016).
[51] T. Liu, D. I. Pikulin, and M. Franz, Phys. Rev. B **95**, 041201 (2017).
[52] A. Rycerz, J. Tworzydlo, and C. W. J. Beenakker, Nat. Phys. **3**, 172 (2007).
[53] D. Xiao, W. Yao, and Q. Niu, Phys. Rev. Lett. **99**, 236809 (2007).
[54] A. Vaezi, N. Abedpour, R. Asgari, A. Cortijo, and M. A. H. Vozmediano, Phys. Rev. B **88**, 125406 (2013).
[55] T. Cao, G. Wang, W. Han, H. Ye, C. Zhu, J. Shi, Q. Niu, P. Tan, E. Wang, B. Liu, and J. Feng, Nat. Commun. **3**, 887 (2012).
[56] J. Kim, C. Jin, B. Chen, H. Cai, T. Zhao, P. Lee, S. Kahn, K. Watanabe, T. Taniguchi, S. Tongay, M. F. Crommie, and F. Weng, arXiv:1612.05359.
[57] P. V. Buividovich, Nucl. Phys. A **925**, 218 (2014).
[58] M. Puhr and P. V. Buividovich, Phys. Rev. Lett. **118**, 192003 (2017).
[59] Z. V. Khaidukov and M. A. Zubkov, Phys. Rev. D **95**, 074502 (2017).
[60] K. G. Wilson, Phys. Rev. D **10**, 2445 (1974).
[61] T. DeGrand and C. DeTar, *Lattice methods for quantum chromodynamics* (World Scientific, New Jersey, 2006).
[62] C. Gattringer and C. B. Lang, *Quantum chromodynamics on the lattice* (Springer-Verlag, Berlin, 2010).
[63] H. B. Nielsen and M. Ninomiya, Phys. Lett. B **105**, 219 (1981).
[64] P. H. Ginsparg and K. G. Wilson, Phys. Rev. D **25**, 2649 (1982); D. B. Kaplan, Phys. Lett. B **288**, 342 (1992).
[65] F. D. M. Haldane, Phys. Rev. Lett. **93**, 206602 (2004).
[66] B. A. Bernevig and T. L. Hughes, *Topological insulators and topological superconductors* (Princeton University Press, Princeton, 2013).
[67] M. A. Metlitski and A. R. Zhitnitsky, Phys. Rev. D **72**, 045011 (2005).

[68] G. M. Newman and D. T. Son, Phys. Rev. D **73**, 045006 (2006).
[69] D. E. Kharzeev and H. U. Yee, Phys. Rev. D **83**, 085007 (2011).
[70] A. A. Burkov, M. D. Hook, and L. Balents, Phys. Rev. B **84**, 235126 (2011).
[71] Z.-M. Huang, J. Zhou, and S.-Q. Shen, Phys. Rev. B **96**, 085201 (2017).